Shaping of PWM Converter Admittance for Stabilizing Local Electric Power Systems

Byeong-Heon Kim, *Student Member, IEEE*, and Seung-Ki Sul, *Fellow, IEEE*

Abstract—This paper suggests the concept of shaping the pulsewidth-modulated (PWM) converter admittance. The analytic admittance matrix equation, which is derived from the small signal model of a PWM converter, is formulized. Based on the damping coefficient and the natural frequencies of phase-locked loop and dc voltage loop, the variations in admittance frequency responses are discussed. In addition, the frequency response can be adjusted through pole placement using the gain of the current controller. The controller gain for a stable operation is designed by detailed understanding of the frequency response shape. Furthermore, to stabilize the local electric power systems (EPSs) that invoke instability through the interaction between constant power load PWM converters, the admittance shaping loop is utilized for the distributed generator PWM converters. Through computer simulation and hardware experiments, the proposed shaping guidance can effectively stabilize local EPS.

Index Terms—Admittance matrix, admittance shaping loop, grid voltage stability.

I. INTRODUCTION

RECENTLY, there has been growing concern for the stability of local electric power systems (EPSs) on a distribution line as distributed generators (DGs) or local loads based on pulsewidth-modulated (PWM) converters have been penetrated. The constant power load (CPL) with PWM converter could be a factor for the instability due to the negative incremental input impedance [1], [2]. Although each CPL with converter has been designed to guarantee a stable EPS operation where CPL is connected, the parallel operation of such CPLs makes the local EPS grid voltage unstable [3].

To maintain the transformer capacity and transmission/distribution line in the present, the installation of PWM converters-based DGs is getting popular. Since these DGs could be coupled to the load in distribution line closely, the parallel operations of converters with their loads are becoming increasingly common. The parallel operation of PWM converters tied to a distribution line could invoke

unexpected interference among converters as the local EPS distribution line has a different source impedance than a strong grid, which looks like an ideal voltage source [3], [4]. Nowadays, with the increase in DGs, the distribution line stability of local EPS equipped with multiple converters is more important.

The impedance-based analysis can be a practical method used to analyze the local EPS stability, and has been successfully used in dc systems [2]. The electrical power system can be characterized by input-output relationships, like impedance or admittance [5]. The addition of an extra unit to the local EPS can be treated as a simple additional impedance or admittance to the existing system. The admittance matrix is analytically obtained by a small signal modeling with an average model concept [2], [6], [7]. The admittance shape had been studied in [6], but the integral gain of the controller was not considered even though it could cause severe instability problems. Much research has concentrated on the admittance variation according to the controller gains, but the authors believe that an intuitive guide for designing the frequency response of the admittance matrix is still missing. The instability phenomena of paralleled CPLs were studied in [3], but there is insufficient literature that considers the stabilizing effect through installing the DG, such as the Photovoltaic (PV) generation unit, battery energy storage system, or active damper circuit to distribution line of local EPS.

In this paper, the admittance matrix model is derived considering the practical implementation of the PWM converter. Although the proposed idea from this paper can be extended to general local EPS equipped with multiple PMW converters, the scope of this paper is limited to PWM converters interfacing the CPL or PV generators that operate at unity power factor to facilitate the understanding of the admittance shaping concept. The variations of frequency response in the admittance matrix are interpreted by control design factors, such as control bandwidth and damping coefficient. As the phase-locked loop (PLL) or dc-link voltage controller would be designed to have second-order low-pass filter characteristics, the natural frequency and damping coefficient of the controllers can intuitively guide the frequency response of admittance. In conjunction with this understanding, the controller design guide is proposed. The unstable load system reported in [3] could be stabilized by adjusting the controller gain according to the proposed design guidance. In addition, an impedance shaping technique for the PV generation unit or active damper is proposed to effectively stabilize the voltage at the point of common coupling (PCC), even though the PV

(a)

(b)

Fig. 1. (a) Small signal representation of an inverter-grid system. (b) Equivalent feedback system.

Fig. 2. Block diagram of control system for CPL or PV generation unit.

generation power capability is much smaller than the total load of local EPS.

II. STABILITY-ORIENTED ADMITTANCE SHAPING WITH TUNING CONTROLLER

A. Impedance-Based Analysis Using Generalized Nyquist Stability Criterion

In this section, the method to analyze system stability is reviewed. To analyze the grid-connected converter stability, an impedance (or admittance)-based analysis can be utilized. The subsystem representing source can be modeled as the Thevenin equivalent circuit, and the subsystem representing the CPL or PV generating unit can be modeled as the Norton equivalent circuit as shown in Fig. 1(a) [8]. The whole system can be represented alternatively as a closed-loop feedback system as shown in Fig. 1(b). The feedback system loop can be analyzed instead of studying the local EPS stability.

In d-q impedance analysis, the system becomes a multi-input multi-output (MIMO). To analyze the MIMO system stability, the roots of the closed-loop characteristic equation in the following could be studied:

$$\det(\mathbf{I} + \mathbf{Z}_g \mathbf{Y}_o) = 0. \qquad (1)$$

Alternatively, the generalized Nyquist stability criterion represents stability by a graphical curve on a complex plane [9], [10]. According to the generalized Nyquist stability criterion, the feedback system is stable *if and only if* the Nyquist curve of (1) does not encircle the origin.

To obtain the admittance matrix of PWM converters, the small signal models have been quantified by an averaged model [2], [3], [6], [11], [12]. In this paper, the output voltage of the converter was directly used to derive the averaged model, while the power equation was used to model the dc system as in [6] and [11]. If the carrier wave for PWM proportionally adjusted according to dc-link voltage, the output voltage of the PWM converter can be accurately synthesized regardless of dc-link voltage variation. In order to consider the
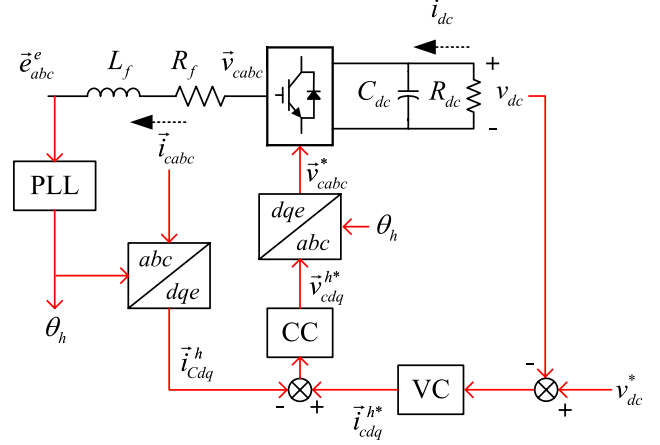
PLL dynamics, the system and converter coordinates can be separated [6], [13], [14]. The delay due to PWM and digital control can also be considered. However, this paper assumes that this delay can be effectively compensated for with a proper algorithm such as the one proposed in [15], and hence this delay has been neglected.

B. Analysis of Small Signal Model According to Controller Gains

The block diagram of a controlled system can be represented in Fig. 2. The dc-link voltage control is constructed while considering the CPL or PV generation unit. For a CPL and DG based on the PV panel, the converter has been assumed to control the power factor as unity. Under this assumption, the output admittances could be diagonalized as in [10] and become (2) and (3)

$$\mathbf{Y}_{cc} = \begin{bmatrix} g_{Icc}^{-1}(1 - a_{ce}) & 0 \\ 0 & g_{Icc}^{-1} \end{bmatrix} \qquad (2)$$

$$\mathbf{Y}_{o} = \begin{bmatrix} g_{Icc}^{-1}(1 - a_{ce}) & 0 \\ 0 & (g_{Icc} + g_{Icl})^{-1} \end{bmatrix} \qquad (3)$$

$$g_{Icc} = \frac{1}{s}[L_f s^2 + (R_f + k_{pc})s + k_{ic}] \qquad (4)$$

$$a_{ce} = (T_c I_{cq}^e + V_{cq}^e)\frac{k_{pp}s + k_{ip}}{s^2 + E_q^e k_{pp}s + E_q^e k_{ip}} \qquad (5)$$

$$g_{Icl} = T_c(1 + a_{oir})^{-1}a_{oi} \qquad (6)$$

$$a_{oir} = \frac{1}{g_{DC}}\frac{3}{2}T_c T_v I_{cq}^e \qquad (7)$$

$$a_{oi} = \frac{1}{g_{DC}}\frac{3}{2}(V_{cq}^e - I_{cq}^e T_c)T_v \qquad (8)$$

$$g_{DC} = C_{dc}V_{dc}s + \frac{2}{R_{dc}}. \qquad (9)$$

In the aforementioned equations, T_{pll}, T_c, and T_v represent the transfer functions of the proportional-integral (PI) controller of PLL, ac current regulator, and dc voltage regulator, respectively. The proportional gain of each controller is defined as k_{pp}, k_{pc}, and k_{pv}. The integral gain of each controller is
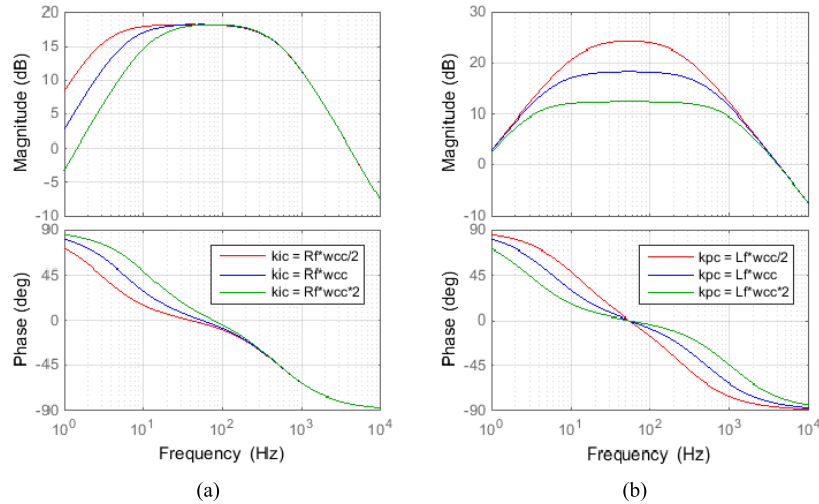
Fig. 3.   Frequency response of (10) according to the control parameter of the current regulator.
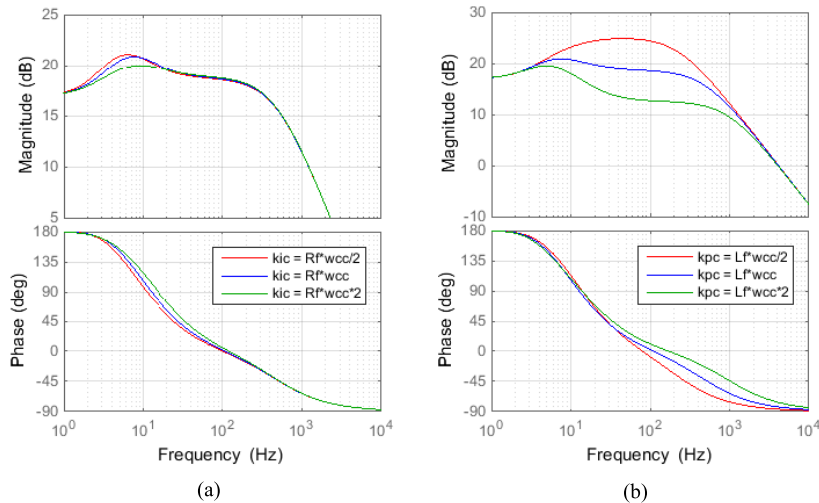
Fig. 4. qq-admittance according to the control parameter of the current regulator.

defined as k_{ip}, k_{ic}, and k_{iv}. I^e_{cq} and V^e_{cq} stand for the operating point of active current and active voltage, respectively. E^e_q represents the peak magnitude of the grid phase voltage. L_f and R_f stand for the inductance and resistance of the filter. C_{dc} and R_{dc} stand for the dc link capacitance and dc load resistance. Finally, the complex variable s is the Laplace transform variable.

The current controller affects the overall functions in (2) and (3). The PLL gains affect a_{ce}. The feedback loop from the grid voltage to the d-axis current reference, such as anti-islanding functionality, is not constructed. In this case, the PLL affects only the dd-admittance. The gains of the dc voltage controller affect g_{Icl}, as seen in (3), and shape the qq-admittance.

If only the current control loop is considered, the output admittance becomes g^{-1}_{Icc}. This can be asymptotically represented as

$$g^{-1}_{Icc} = \frac{s}{L_f s^2 + (R_f + k_{pc})s + k_{ic}}$$
$$\approx \frac{s}{L_f(s + \omega_f \frac{\rho_{ic}}{\rho_{pc}})(s + \omega_{cc}\rho_{pc})}. \quad (10)$$

The gains of the current controller are designed as $k_{pc} = \rho_{pc}L_f\omega_{cc}$ and $k_{ic} = \rho_{ic}R_f\omega_{cc}$. If both ρ_{pc} and ρ_{ic} are set to 1, the transfer function of the current control becomes the first-order low-pass filter with bandwidth ω_{cc}. In (10), ω_f represents the pole set by the filter parameter. From (10), k_{ic} contributes to the migration of the filter pole, ω_f, and k_{pc} contributes to the migration of both ac current dynamics poles. The bandwidth of the current control can be determined by the switching frequency of the converter. The bandwidth is set below 1/6 the switching frequency in a practical sense [16].

Fig. 3 shows the Bode plot of the admittance in (10), which determines the dynamics of output admittance, except for qq-admittance in (2), without PLL dynamics. The results confirm the description reported in the previous paragraph. Fig. 4 shows the qq-admittance with the dc voltage controller. Due to the dc voltage control effect, the phase response is alleviated around the pole by the filter parameters.

In [3] and [8], the admittance shape was analyzed according to the proportional and integral gains of the PLL and dc voltage regulator. This made the interpretation of the admittance
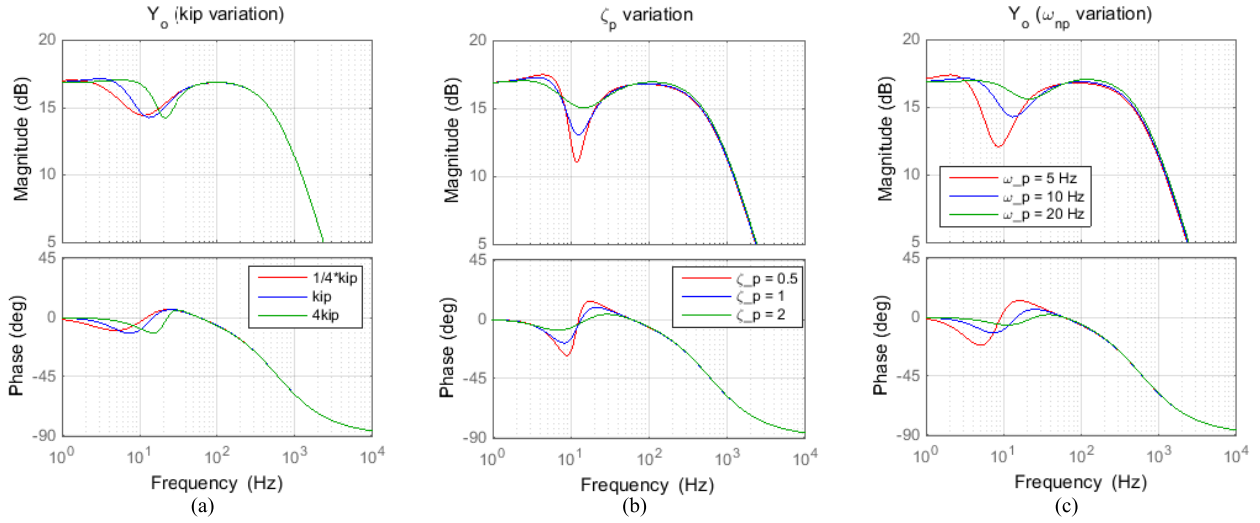
Fig. 5.   *dd*-admittance of the converter according to the control parameters of the PLL.
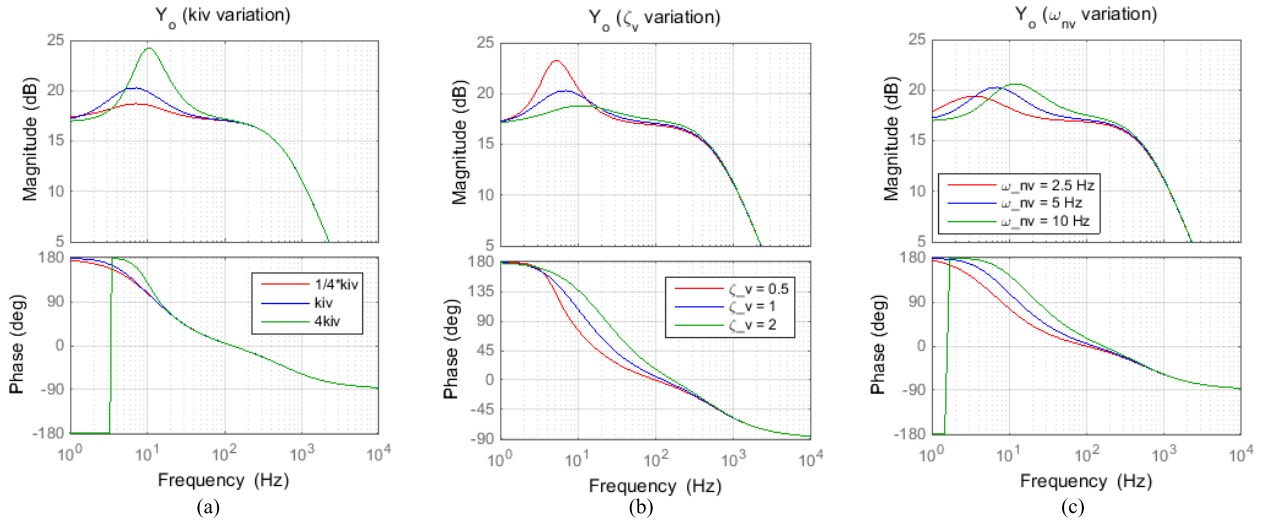
Fig. 6.   *qq*-admittance of the converter according to the control parameters of the dc-link voltage regulator.

frequency response difficult. However, the PI controller gains of the PLL and dc voltage regulator could be designed based on the second-order filter characteristics. Furthermore, the variation of the gains would be considered equivalent to the variation of the natural frequency and the damping coefficient. The natural frequency determines the location of the pole, while the damping coefficient determines the magnitude of the peak at the natural frequency. The damping coefficient relates to phase variation, so an underdamped design varies the phase dramatically. If gains are overdamped, the interval of phase variation is enlarged.

The input-output transfer function of PLL and dc voltage regulation with PI controller can be designed as [17]

$$\frac{\theta_h}{\theta} = \frac{E_q^e \left(k_{pp}s + k_{ip} \right)}{s^2 + E_q^e k_{pp}s + E_q^e k_{ip}} = \frac{2\zeta_p \omega_{np}s + \omega_{np}^2}{s^2 + 2\zeta_p \omega_{np}s + \omega_{np}^2} \quad (11)$$

$$\frac{v_{dc}}{v_{dc}^*} = \frac{C_v^{-1} k_{pv}s + C_v^{-1} k_{iv}}{s^2 + C_v^{-1} k_{pv}s + C_v^{-1} k_{iv}} = \frac{2\zeta_v \omega_{nv}s + \omega_{nv}^2}{s^2 + 2\zeta_v \omega_{nv}s + \omega_{nv}^2} \quad (12)$$

where $C_v = 2C_{dc}V_{dc0}/3E_q^e$. V_{dc0} stands for the operating point of dc voltage. ω_{np} and ω_{nv} stand for the natural frequencies of PLL and dc voltage regulator, respectively. ζ_p and ζ_v stand for the damping coefficient of each regulator.

The natural frequency is associated with I gain. The damping coefficient is proportional to the P gain and inversely proportional to the square root of I gain. Since (11) is included in (5), the variation of (11) according to ω_{np} or ζ_p can directly affect the admittance shape. On the other hand, the relationship between (6) and (12) is not clear. However, the admittance matrix (3) can be shaped by properly designing ω_{nv} and ζ_v as in (12).

Figs. 5 and 6 show the admittance variation according to the natural frequencies and damping coefficients for a CPL. For comparison, the results show the variation of I gain. Because the variation of P gain is the same as that of the damping coefficient, the related results are not displayed. In Fig. 5, as the natural frequency of PLL increases, the location of
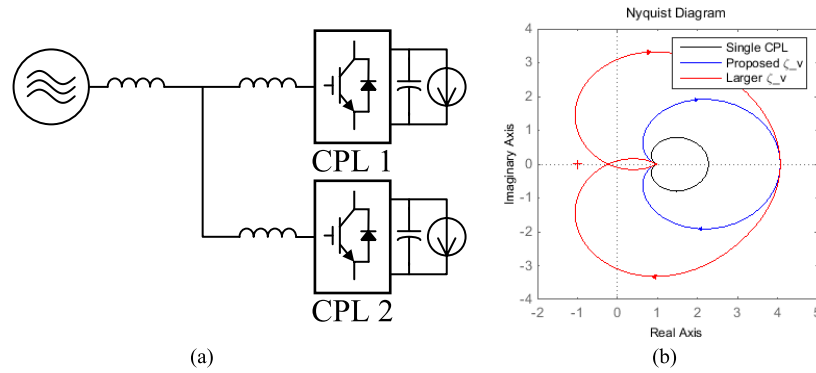
Fig. 7. (a) System configuration in time-domain circuit simulation. (b) Generalized Nyquist curves.
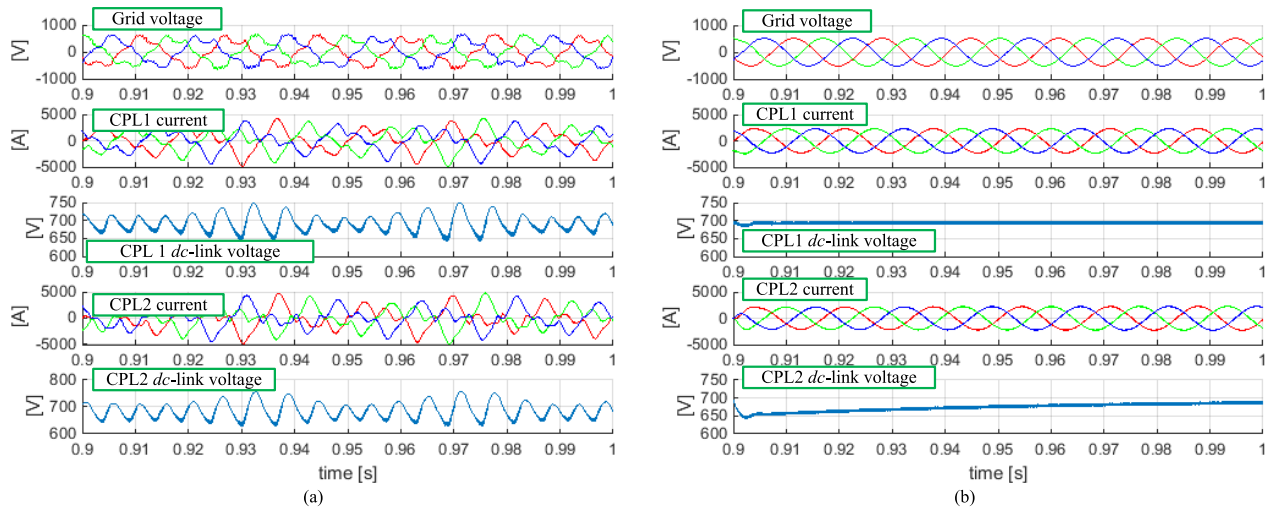
Fig. 8. Results of time-domain simulation for parallel CPL. (a) Larger damping coefficient. (b) Proposed damping coefficient.

the phase change is moving upward. The PLL affects only dd-admittance, which is expected by (2) and (3). As the damping coefficient becomes smaller, the magnitude valley is deeper and the phase response slope is steeper. However, if I gain is adjusted, both the natural frequency and damping coefficient are changed so that the design guide cannot be obtained. In Fig. 5, the control parameters of dc voltage regulation show similar dynamics and the dc voltage regulator affects qq-admittance as described by (3). Although g_{Icl} has complicated interactions with other controllers, the phase and magnitude responses are forecasted by the natural frequency and damping coefficient of the voltage regulator.

From [18]–[21], the damping coefficient of PLL severely affects the stability of the system under weak grid conditions. Compared with critical damping, an extremely underdamped or overdamped design can invoke instability. The damping coefficient of PLL is set at the recommended 0.707, which corresponds to the critical damping.

To alleviate magnitude peaking for the dc voltage regulator, the damping coefficient is to be set between 0.707 and 3. If the damping coefficient is set over 3, the slope of the phase response in the frequency domain becomes too small. On the other hand, the phase response dramatically varies as
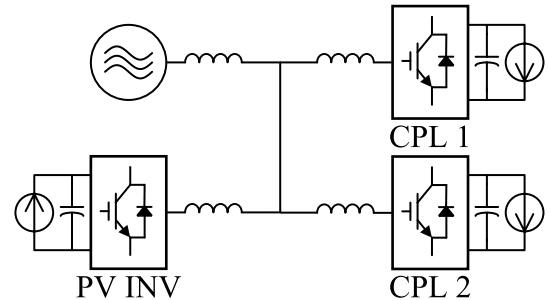
Fig. 9. System configuration in time-domain circuit simulation.

the damping coefficient decreases. However, the magnitude in the frequency domain has large peak value. The natural frequency should be carefully designed while considering physical parameters, such as sampling frequency, the amount of disturbance, and so on. For both PLL and dc voltage controllers, the natural frequency would be set below one-third of grid frequency.

C. Instability Caused by Interaction Between Converters

As reported in [3], the parallel operation of converters connected to CPL, originally designed to guarantee the stable
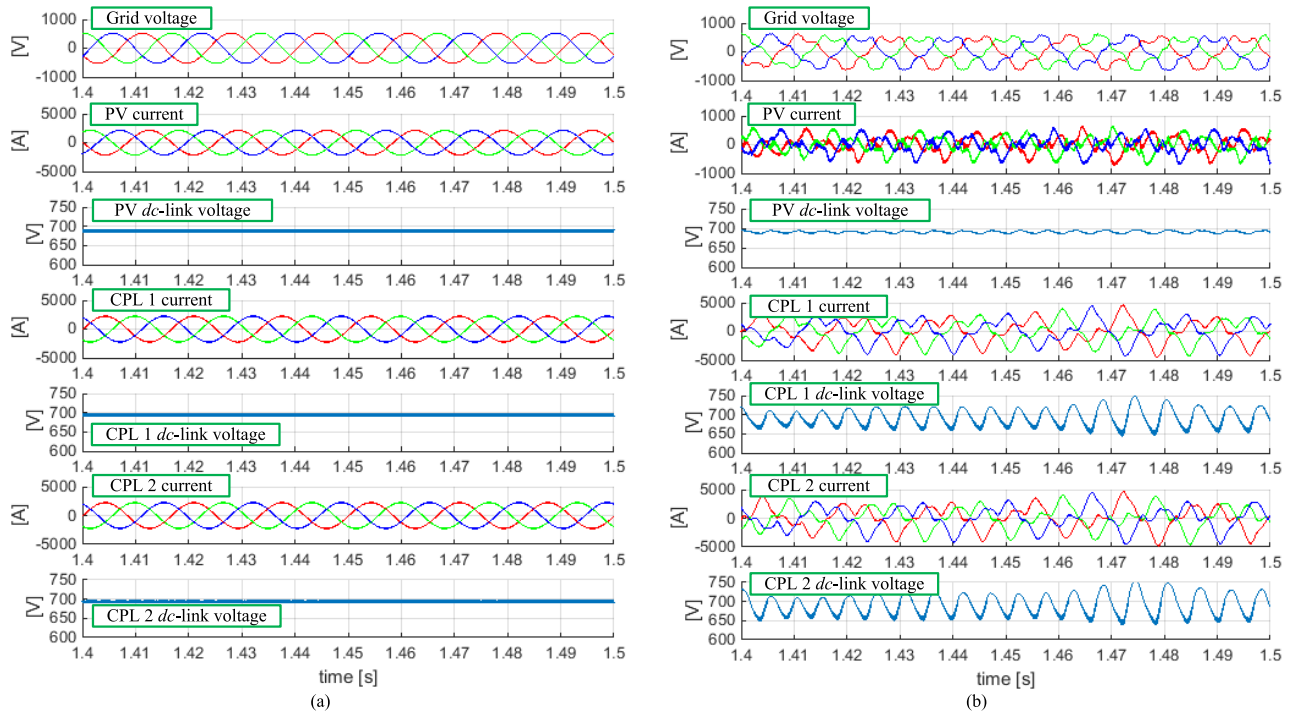
Fig. 10. Results of time-domain simulation for parallel CPLs and a PV generator. (a) 100% power generation. (b) 10% power generation.

operation of the single converter itself, can induce instability due to the interaction of converters. Fig. 7(a) shows the parallel operation system configuration of CPLs.

Although each converter is designed to be stable, the large damping coefficient can lead to instability due to the insufficient phase margin at midfrequency ranges. If the proposed damping coefficient is adopted, the parallel operation becomes stable under the same grid impedance. Fig. 7(b) shows the generalized Nyquist curves. For the single CPL and paralleled CPLs with the proposed gain ($\zeta_v = 3$), the Nyquist curves do not encircle the origin. However, for the paralleled CPLs with a larger damping coefficient ($\zeta_v = 8$), the Nyquist curve encircles the origin and implies instability in the entire system. Fig. 8 shows the results of the time-domain simulation. The parameters for the simulation are listed in Table I.

III. STABILITY-ORIENTED ADMITTANCE SHAPING WITH ACTIVE DAMPING

If the controller of the load cannot adjust, the additional generation unit can alleviate the possibility of instability. As shown in Fig. 9, one PV generation unit is assumed to have the same power capacity and control scheme with load installed to the local EPS distribution line. The only difference between the load and PV unit is the direction of power flow. Because the Maximum Power Point Tracking (MPPT) algorithm works in longer periods, the MPPT is neglected in small signal modeling. The q-component of the PV converter admittance has the same magnitude and opposite phase compared with admittance of a load converter at the midfrequency range. As a result, the admittance of a load converter can be canceled out by one PV converter with the same power capacity. As depicted in Fig. 10(a), with

TABLE I
PARAMETERS IN SIMULATION

Rated power	1 MW (1 p.u.)
Grid voltage (line-to-line)	380 V_{rms} (1 p.u.)
Grid frequency (base frequency, ω_b)	60 Hz
Grid impedance	0.05 p.u.
Output filter inductance	0.15 p.u.
dc voltage	690V
dc-link capacitance	36.7 mF
ω_{np}	$2\pi \times 10$ rad/s
ζ_p	1
ω_{cc}	$10\,\omega_b$
ω_{nv}	$1/3\,\omega_b$

the additional PV generation unit, the system with the same control parameter in Fig. 8(a) can be stabilized. However, if the generation power of the PV unit is reduced due to the shading effect or solar irradiation variation, the PV converter cannot stabilize the system [Fig. 10(b)].
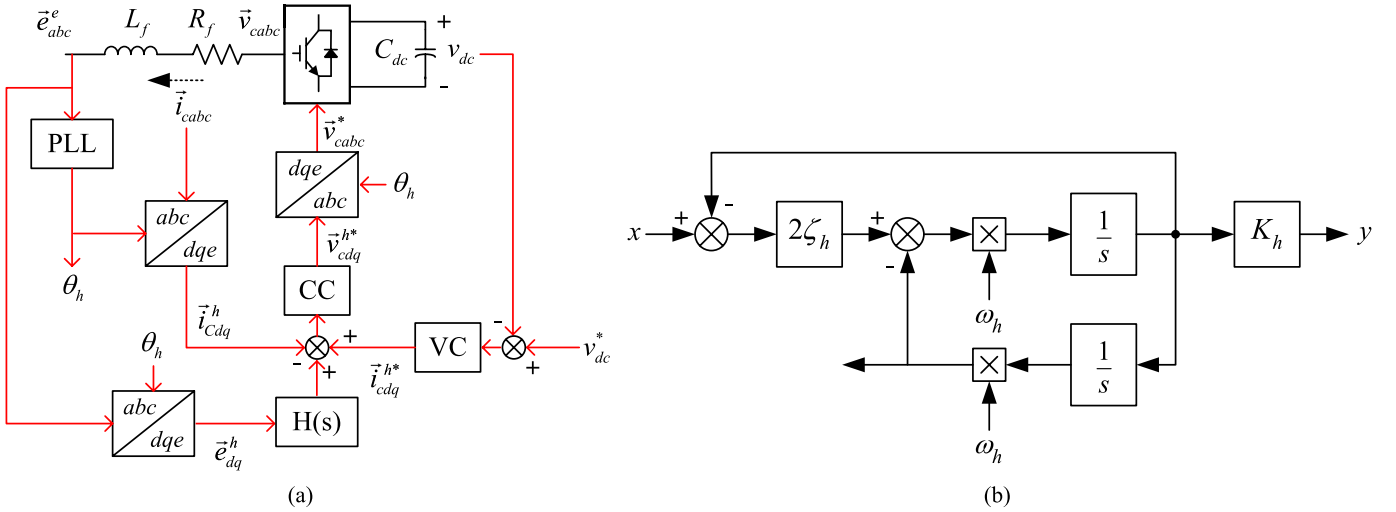
Fig. 11.   (a) Admittance shaping loop. (b) Bandpass filter–SOGI structure.
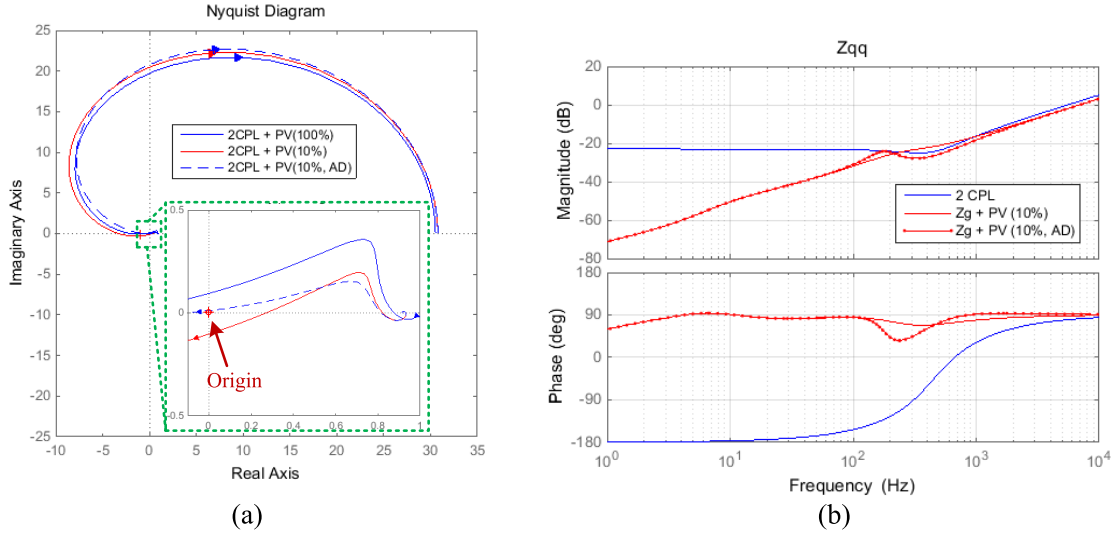
Fig. 12.   (a) Generalized Nyquist curves. (b) Bode plot of qq-impedance.

To provide a stabilizing effect on an unstable operation even under irradiation reduction, the admittance shaping loop is constructed according to the PV converter. To directly shape the PV converter admittance, the feedback loop from grid voltage to converter current could be designed. Fig. 11(a) shows the control scheme with an impedance shaping loop. To shape the frequency response at the midfrequency range, various transfer functions can be applied. For example, the bandpass filter in (13) can be utilized similar to the active damping in [9] that relieves subsynchronous interactions. To realize the bandpass filter, the second-order generalized integrator (SOGI) structure in Fig. 11(b) is adopted. If the frequency region of instability is changed, various types of shaping loops can be adopted

$$H(s) = \begin{bmatrix} 0 & 0 \\ 0 & K_h \dfrac{2\zeta_h \omega_{nh} s}{s^2 + 2\zeta_h \omega_{nh} s + \omega_{nh}^2} \end{bmatrix}. \quad (13)$$

If the feedback loop with (13) is constructed, the output admittances are changed to (14). As shown in the following, the qq-admittance can be adjusted directly by the feedback of the grid voltage to converter current through the bandpass filter:

$$\mathbf{Y}_o = \begin{bmatrix} g_{Icc}^{-1}(1-a_{ce}) & 0 \\ 0 & (g_{Icc}+g_{Icl})^{-1}(1-T_c(1+a_{\text{oir}})^{-1}H(s)) \end{bmatrix}. \quad (14)$$

Although the generating power of PV is reduced to 10%, the system can be stabilized with the admittance shaping loop. The generalized Nyquist curve in Fig. 12(a) shows that the stability margin has been increased by active damping, and the system becomes stable. Fig. 12(b) shows the qq-impedance variation by loop shaping. With loop shaping, as the grid dd-impedances decreases, the magnitude overlapping has disappeared. This can also be verified by time-domain simulations as shown in Fig. 13.
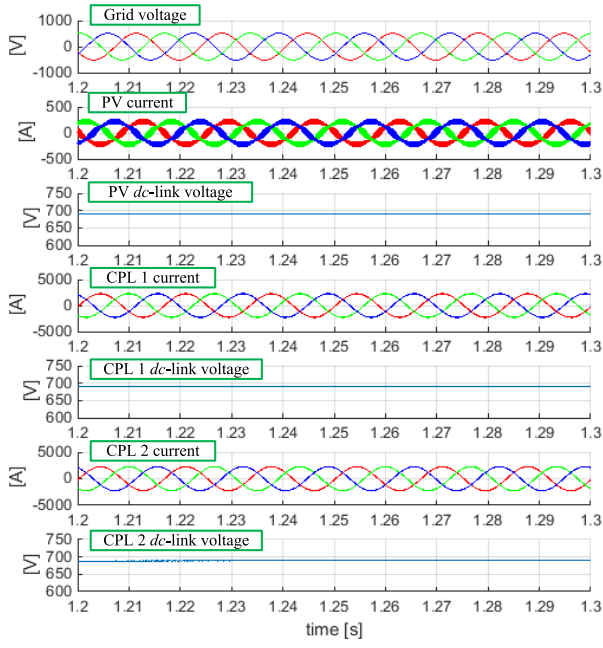
Fig. 13. Results of time-domain simulation for parallel CPLs and a PV generator (10% power generation, active damping).

TABLE II
PARAMETERS IN EXPERIMENT

Rated power	3 kW
Grid voltage (line-to-line)	220 V_{rms}
Grid frequency	60 Hz
Grid inductance	4 mH
Output filter inductance	1.9 mH
dc voltage	350V
dc-link capacitance	2 mF
ω_{cc}	10 ω_b
ω_{np}	$2\pi \times 10$ rad/s
ζ_p	1

IV. EXPERIMENTAL RESULTS

Hardware experiments were carried out to verify the proposed idea and discussion. The circuit specified in Figs. 7 and 9 is constructed in small scale. The parameters for the experimental setup are listed in Table II.

As the CPLs with the proposed gain are operated in parallel, the system can be operated stably [Fig. 14(a) and (c)]. However, as the damping coefficient increases, the grid voltage contains oscillations [Fig. 14(b) and (d)]. Due to the
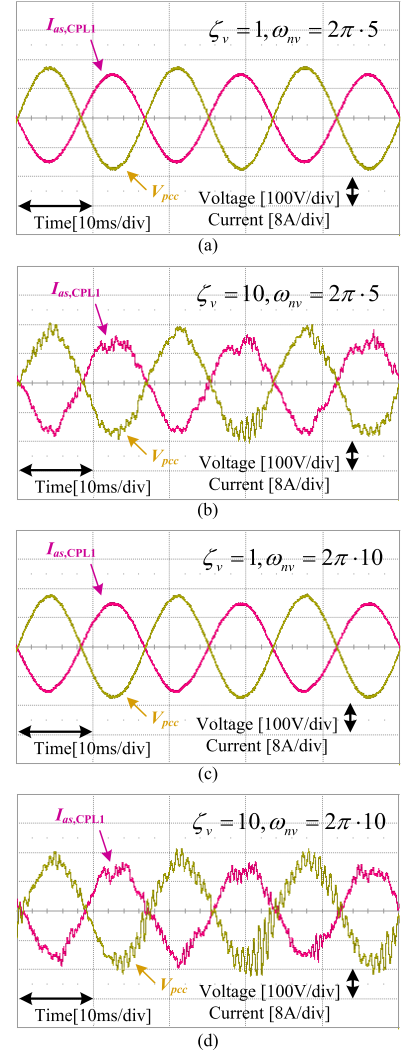
Fig. 14. Experimental results with different control parameters–parallel CPLs.

insufficient phase margin at the midfrequency range from the large damping coefficient, the midfrequency oscillation (about 180 Hz) is observed. High-frequency oscillations (about 1 kHz) from unpredictable parasitic components in the system are also seen.

Fig. 15 shows the results with the admittance shaping loop where the generation power by PV unit is assumed to be zero. In the worst case, the irradiation on the PV panel could be entirely shaded so that the generating power of the PV unit becomes zero. This worst case scenario was assumed for the experiment. The active damping can stabilize the system operation even in this worst case. The active damping is designed based on previous result observations. The midfrequency oscillation can be suppressed by the bandpass filter, whose center frequency is set to 180 Hz in impedance shaping loop. High-frequency oscillation due to parasitic components can also be suppressed by an additional paralleled bandpass filter of 1 kHz. Compared with the results in Fig. 14(b) and (d), the PV unit significantly reduces the oscillations of the grid voltage although the average power supply of the PV unit is zero. Even though the current control bandwidth is set below
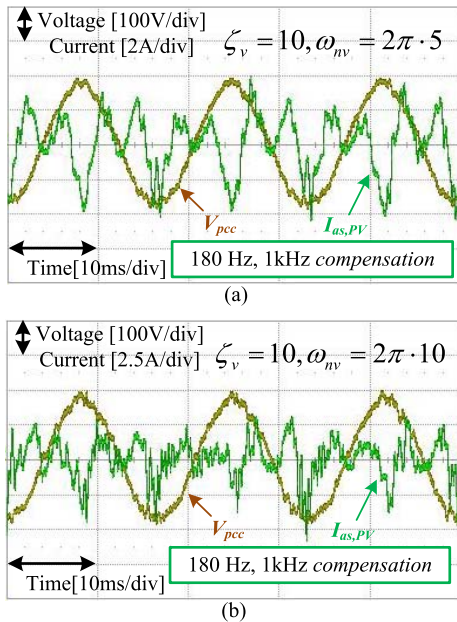
Fig. 15. Experimental results with different control parameters–admittance shaping by PV generation unit without power generation.

the oscillation frequency 1 kHz, the grid voltage distortion could be relieved conspicuously by the admittance shaping loop.

V. CONCLUSION

This paper proposes the design guidance to shape the admittance matrix of PWM converter for CPL or DG. To obtain the admittance matrix, the practical compensation algorithms of the PWM converter to synthesize proper output voltage are considered. Assuming the unity power factor operation, the diagonal admittance matrix could be obtained and the analytic equations derived. The design guide for the shaping frequency response of the admittance matrix is based on the damping coefficient and the natural frequency of the PLL and dc voltage controller. Both parameters can provide intuitive information to shape the frequency response magnitude or phase. The changing gains of the current controller can be interpreted as pole placement. In conjunction with this understanding, the controller design guidance has been proposed.

The unstable load system proposed in another paper could be stabilized by adjusting the controller gain to the values according to the guides in this paper. Stabilization through the PV generation unit with paralleled CPL has been discussed for future local EPS construction. The admittance shaping loop on the PWM converter of the PV generation unit is also proposed where the system can be stabilized through a proposed feedback loop, even with low power generation. In experimental tests, the admittance shaping loop can effectively stabilize the voltage at the PCC even without the power generation of the PV system.

VI. ACKNOWLEDGMENT

REFERENCES

[1] M. Belkhayat, "Stability criteria for AC power systems with regulated loads," Ph.D. dissertation, Dept. Eng., Electron. Electr., Purdue Univ., West Lafayette, IN, USA, Dec. 1997.

[2] B. Wen, D. Boroyevich, R. Burgos, P. Mattavelli, and Z. Shen, "Small-signal stability analysis of three-phase AC systems in the presence of constant power loads based on measured $d-q$ frame impedances," *IEEE Trans. Power Electron.*, vol. 30, no. 10, pp. 5952–5963, Oct. 2015.

[3] C. Wan, M. Huang, C. K. Tse, and X. Ruan, "Effects of interaction of power converters coupled via power grid: A design-oriented study," *IEEE Trans. Power Electron.*, vol. 30, no. 7, pp. 3589–3600, Jul. 2015.

[4] D. Dong, B. Wen, P. Mattavelli, D. Boroyevich, and Y. Xue, "Grid-synchronization modeling and its stability analysis for multi-paralleled three-phase inverter systems," in *Proc. 28th Annu. IEEE Appl. Power Electron. Conf. Expo. (APEC)*, Mar. 2013, pp. 439–446.

[5] S. Pika and S. Danielsen, "Understanding of the stability criterion for a double-feedback loop system," in *Proc. Elect. Syst. Aircraft, Railway Ship Propuls. (ESARS)*, 2010, pp. 1–5.

[6] L. Harnefors, M. Bongiorno, and S. Lundberg, "Input-admittance calculation and shaping for controlled voltage-source converters," *IEEE Trans. Ind. Electron.*, vol. 54, no. 6, pp. 3323–3334, Dec. 2007.

[7] J. Sun, "Small-signal methods for AC distributed power systems— A review," *IEEE Trans. Power Electron.*, vol. 24, no. 11, pp. 2545–2554, Nov. 2009.

[8] J. Sun, "Impedance-based stability criterion for grid-connected inverters," *IEEE Trans. Power Electron.*, vol. 26, no. 11, pp. 3075–3078, Nov. 2011.

[9] S. Skogestad and I. Postlethwaite, "Elements of linear system theory," in *Multivariable Feedback Control: Analysis and Design*. New York, NY, USA: Wiley, 2001.

[10] R. Burgos, D. Boroyevich, F. Wang, K. Karimi, and G. Francis, "On the AC stability of high power factor three-phase rectifiers," in *Proc. IEEE Energy Convers. Congr. Expo. (ECCE)*, Sep. 2010, pp. 2047–2054.

[11] X. Wang and W. Freitas, "Impact of positive-feedback anti-islanding methods on small-signal stability of inverter-based distributed generation," *IEEE Trans. Energy Convers.*, vol. 23, no. 3, pp. 923–931, Sep. 2008.

[12] A. A. A. Radwan and Y. A. R. I. Mohamed, "Analysis and active-impedance-based stabilization of voltage-source-rectifier loads in grid-connected and isolated microgrid applications," *IEEE Trans. Sustain. Energy*, vol. 4, no. 3, pp. 563–576, Jul. 2013.

[13] K. M. Alawasa, Y. A. R. I. Mohamed, and W. Xu, "Modeling, analysis, and suppression of the impact of full-scale wind-power converters on subsynchronous damping," *IEEE Syst. J.*, vol. 7, no. 4, pp. 700–712, Dec. 2013.

[14] B. Wen, D. Boroyevich, P. Mattavelli, Z. Shen, and R. Burgos, "Influence of phase-locked loop on input admittance of three-phase voltage-source converters," in *Proc. 28th Annu. IEEE Appl. Power Electron. Conf. Expo. (APEC)*, Mar. 2013, pp. 897–904.

[15] B.-H. Bae and S.-K. Sul, "A compensation method for time delay of full-digital synchronous frame current regulator of PWM AC drives," *IEEE Trans. Ind. Appl.*, vol. 39, no. 3, pp. 802–810, May/Jun. 2003.

[16] G. Ellis, "Delay in digital controllers," in *Control System Design Guide: A Practical Guide*. London, U.K.: Elsevier, 2004.

[17] S.-K. Sul, "Design of regulators for electric machines and power converters," in *Control of Electric Machine Drive Systems*. Piscataway, NJ, USA: IEEE Press, 2011.

[18] B. Wen, D. Boroyevich, P. Mattavelli, R. Burgos, and Z. Shen, "Modeling the output impedance negative incremental resistance behavior of grid-tied inverters," in *Proc. 29th Annu. IEEE Appl. Power Electron. Conf. Expo. (APEC)*, Mar. 2014, pp. 1799–1806.

[19] B. Wen, D. Boroyevich, R. Burgos, P. Mattavelli, and Z. Shen, "Analysis of D-Q small-signal impedance of grid-tied inverters," *IEEE Trans. Power Electron.*, vol. 31, no. 1, pp. 675–687, Jan. 2016.

[20] B. Wen, D. Dong, D. Boroyevich, P. Mattavelli, R. Burgos, and Z. Shen, "Impedance-based analysis of grid-synchronization stability for three-phase paralleled converters," *IEEE Trans. Power Electron.*, vol. 31, no. 1, pp. 26–38, Jan. 2016.

[21] T. Messo, J. Jokipii, A. Mäkinen, and T. Suntio, "Modeling the grid synchronization induced negative-resistor-like behavior in the output impedance of a three-phase photovoltaic inverter," in *Proc. 4th IEEE Int. Symp. Power Electron. Distrib. Generat. Syst. (PEDG)*, Jul. 2013, pp. 1–7.

Byeong-Heon Kim (S'11) was born in South Korea in 1988. He received the B.S. and M.S. degrees in electrical engineering from Seoul National University, Seoul, South Korea, in 2010 and 2012, respectively, where he is currently pursuing the Ph.D. degree in electrical engineering and computer science.

He was involved in power conditioning system for renewable energy and in machine drive for engine-generator system. His current research interests include control and stability of power conditioning systems.

Seung-Ki Sul (S'78–M'87–SM'98–F'00) received the B.S., M.S., and Ph.D. degrees from Seoul National University, Seoul, South Korea, in 1980, 1983, and 1986, respectively, all in electrical engineering.

He was an Associate Researcher with the Department of Electrical and Computer Engineering, University of Wisconsin–Madison, Madison, WI, USA, from 1986 to 1988. From 1988 to 1990, he was a Principal Research Engineer with LG Industrial Systems Company, Cheongju, South Korea. Since 1991, he has been a Faculty Member with the School of the Electrical and Computer Engineering, Seoul National University, where he is currently a Professor. He has authored over 140 IEEE reviewed journal papers and a total of more than 330 international conference papers in the area of power electronics. He holds 14 U.S. patents, seven Japanese patents, and 11 Korean patents, and granted 38 Ph.D. students under his supervision. His current research interests include control of electrical machines, electric/hybrid vehicles, electric propulsion of ship, and power conditioning system for renewables.

Prof. Sul received many best paper awards from international conferences and journals, including the first and second best paper awards, simultaneously, from the IEEE TRANSACTIONS ON INDUSTRY APPLICATIONS, in 2015. He was the Program Chair of the IEEE PESC in 2006, and the General Chair of the IEEE ECCE-Asia, ICPE, in 2011. In 2015, he served as the President of the Korea Institute of Power Electronics.